ORIGINAL ARTICLE

The Role of Peroxisome Proliferator Activated Receptor γ (PPARγ) Ligands on Foam Cells Formation Derived From Murine Norovirus-1 (MNV-1) Infected Macrophage

Khirun Musa[1], Rafeezul Mohamed[1], Ida Shazrina Ismail[1], Muhammad Amir Yunus[2]

[1] Regenerative Medicine Cluster, Advanced Medical and Dental Institute, Universiti Sains Malaysia, Bertam, 13200 Kepala Batas, Pulau Pinang, Malaysia.
[2] Infectomics Cluster, Advanced Medical and Dental Institute, Universiti Sains Malaysia, Bertam, 13200 Kepala Batas, Pulau Pinang, Malaysia.

ABSTRACT

Introduction: Atherosclerosis is a chronic inflammatory disease initiated by the accumulation of macrophage derived foam cells in the intima layer of artery. In mice model of atherosclerosis, murine norovirus-4 has been shown to accelerate atherogenesis. In cells, lipid biometabolism is regulated by peroxisome proliferator activated receptor γ (PPARγ). Since PPARγ is predominantly expressed in macrophages and mice macrophages are MNV-1 proliferation-permissive host, we hypothesised that PPARγ ligands may regulate atherogenesis. Methods: MNV-1 was generated via RNA-based recovery system and used to infect the RAW 264.7 cells, then subjected to oxidized low-density lipoprotein (oxLDL)-loaded and treated with ciglitazone or 15-deoxy-Delta(12,14)-PGJ(2)(15d-PGJ2). Foam cell formation was evaluated and the MNV-1 infection in all treatments was confirmed using virus titration (50% tissue culture infective dose; TCID50) and polymerase chain reaction (PCR). Results: Increment of lipid droplets was observed in all oxLDL treatment involving MNV-1 infection, ciglitazone or 15d-PGJ2 in the cytosol of RAW 264.7 cells over time compared to non-oxLDL treated cells. From the cholesterol ester (CE) content analysis amongst the oxLDL-loaded cells however, we found MNV-1 did not elicit increment of CE content. Treatment with 15d-PGJ2 resulted in increase of the CE content in oxLDL-treated cells. Interestingly, MNV-1 and ciglitazone had synergistic effect in reducing the CE content in oxLDL-treated cells. Conclusion: oxLDL stimulates foam cells formation in RAW 264.7 cells. However, MNV-1 infection did not contribute to RAW 264.7 cells derived-foam cells formation. On the other hand, 15d-PGJ2 promotes foam cells formation whilst ciglitazone inhibits the formation of foam cells derived from MNV-1-infected macrophages.

Keywords: Atherosclerosis, Ciglitazone, Foam cells, Murine norovirus-1 (MNV-1), 15d-PGJ2

Corresponding Author:
Muhammad Amir Yunus, PhD
Email: amiryunus@usm.my
Tel: +604-5622560

INTRODUCTION

Atherosclerosis is recognised as an inflammatory disease due to hardening and narrowing of the arteries which can lead to various cardiovascular diseases such as myocardial infarction (heart attack), stroke, unstable angina (ischemic heart pain), and sudden cardiac death (1, 2). During early phase of atherogenesis, monocytes migrate from the subendothelial space into the intima layer of arteries where they were further differentiated into macrophages under influence of monocyte colony stimulating factor (M-CSF) (3). The engulfment of oxidized low-density lipoprotein (oxLDL) triggering the exaggeration of cholesterol esterification and disruption cholesterol dispersion causing the deposition of cholesterol ester (CE) storage namely lipid droplets and afterwards promote foam cells formation which act as an integral in the atherosclerosis development (4). Numerous infectious agents have been reported as accelerator for atherogenesis which included *Chylamidiae pneumonia* (5), *Porphyromonas gingivalis* (6), influenza virus (7), cytomegalovirus (8) and human immunodeficiency virus (HIV) (9). Recently, murine norovirus-4 (MNV-4) infections have been reported to stimulate the deposition of atherosclerotic plaque lesion in aortic sinus of Ldlr-/- and ApoE-/- mice, a well-known mouse model for atherosclerosis research (10, 11). MNV-4 infection also boosts the macrophage quantity in the atherosclerotic plaque which corresponds with accumulation of macrophage derived foam cells (10). Moreover, MNV-4 infection also stimulated the secretion of pro-atherogenic cytokines *in vitro* (11).

MNV was initially identified in 2003 and characterised as a single-stranded, positive-sense RNA virus from

Caliciviridae family and the genus of norovirus (12, 13). MNV typically transmitted through faecal-oral route and commonly infected gastrointestinal tract (14). Furthermore, MNV infection is also commonly reported in the specific pathogen free (SPF) facilities in the United States, Canada, Asia and Europe which may influence the outcomes of the on-going research using mice (15, 16). There were four different strains of MNV that have been identified so far namely MNV-2, MNV-3 and MNV-4 which exhibited persistent infections with prolonged faecal shedding in immunocompetent mice, while MNV-1 is transient and displays a short duration infection and typically disappear in the faeces of mice for less than one week (17). MNV is the best model for norovirus studies in *in vitro* systems as it can be propagated in cell culture, specifically with tropism in macrophages and dendritic cells (18).

Peroxisome proliferator activated receptors (PPAR) are ligand activated transcription factors from a subfamily of the nuclear receptor gene family (19, 20). PPARs exist in three different subtypes namely PPARα, PPARδ/β and PPARγ that are resulted from differential splicing (21). PPARs involved in the earliest phase of atherogenesis by modulating the expression of chemokine receptors as well as adhesion molecules in endothelial cell (EC), T cells and monocytes which initiate the inflammatory process (22). Previous study by Li et al., (2004) showed that PPARγ ligands capable of inhibiting atherogenesis in vivo (23). PPARγ agonists increased the expression of the cholesterol transporter namely ATP binding cassette transporter G1 (ABCG1) in primary macrophages and in the hypercholesterolemic mice arterial walls (23). The PPARα, PPARβ, and PPARγ specific agonists also can impede the expression of several genes that associate with the atherogenesis, including vascular cell adhesion molecule (VCAM)-1, monocyte chemoattractant protein (MCP)-1, and IFNγ (23). On the other hand, PPARγ agonists increased the expression of CD36 in macrophages and accelerated the uptake of oxLDL (24). Moreover, intracellular adhesion molecule (ICAM)-1 and VCAM-1 expression is inhibited by troglitazone treatment in human EC (25). Since PPARγ is predominatly expressed in macrophages and there is no report until to date on the role of MNV-1 (short clinical infection) in atherogenesis, the current study was carried out to investigate whether PPARγ ligands (ciglitazone and 15d-PGJ2) may regulate atherogenesis by controlling the formation of foam cells derived from MNV-1 infected macrophages.

MATERIALS AND METHODS

Cells

Murine macrophage cell line (RAW264.7), Baby Hamster Kidney engineered to express T7 RNA polymerase (BSR-T7) cell line and murine microglial cell line (BV2) were obtained as kind gift from Professor Ian Goodfellow, University of Cambridge. The RAW264.7 cell line was maintained in Dulbecco's modified Eagle's medium (DMEM) and supplemented with 10% FBS, 1% penicillin/streptomycin and 1% HEPES (1M). The BV2 cell line was maintained in DMEM supplemented with 10% FBS, 1% penicillin/streptomycin while BSR-T7 cell line was cultured in DMEM supplemented with 10% FBS, 1% penicillin/streptomycin and 0.001% gentamycin (G418). All the cells were incubated at 37°C in 5% CO_2 incubator.

Low density lipoprotein isolation

Whole blood was obtained from healthy donors by qualified personnel (USM/JEPeM/14090330) and stored in BD Vacutainer Lithium Heparin 75 USP units. The plasma was then harvested by centrifugation at 800 x g for 45 minutes at 4°C. Then, 2 ml of the 60% Optiprep (Fresinius Kabi Norge, Norway) were mixed with 8 ml plasma in a new falcon tube to provide 12% of Optiprep (Fresinius Kabi Norge, Norway). In parallel, 6 ml of 6% Optiprep (Fresinius Kabi Norge, Norway) were added to a Beckman tube and the 12% of Optiprep were carefully layered at the bottom of Beckman tube. Next, the tube was centrifuged at 227,694.8 x g for 5 hours and 30 minutes at 16°C using Beckman NVT 65 rotor and a Beckman Optima XL 100 ultracentrifuge (Beckman Coulter Inc., USA). The yellow LDL band was carefully collected and transferred into a new falcon tube (protected from light). The obtained LDL was dialysed against PBS for 48 hours and then subjected to oxidization using CuSO4 for 24 hours at room temperature. Then, the oxLDL were filtered through 0.2 µm membrane filter and dialysed against PBS for 24 hours. Concentration of oxLDL were determined using Nano drop® (Thermo Fischer Scientific Inc., UK) and standardized at 1 mg/ml.

Recovery of recombinant MNV-1 using RNA-based reverse genetics system

RNA-based virus recovery method used in the current study for the recovery of MNV-1 was described in detail by Yunus et al., (2010). Briefly, three types of plasmid were used as template for *in vitro* transcription reaction. These plasmids were the wild type (W/T) plasmid harboring wild-type MNV-1 genome (CW1), the frameshift (F/S) plasmid which is a derivative of W/T plasmid with a frame shift mutation in the NS7 region of MNV genome, resulting in truncated NS7 expression product, and the mut-NS7 plasmid (point mutation has been introduced to NS7 region to produce a mutation in the active site of RNA-dependent RNA polymerase (RdRP)). All the plasmids were linearised using NheI restriction enzyme. Following DNA purification, the linearised plasmids were used as templates in T7 RNA polymerase-based *in vitro* transcription reaction to generate MNV-1 RNA transcripts. Subsequently the transcripts were subjected to enzymatic capping reaction to produce 5'-end capped structure as described in Yunus et al., (2010). One µg of the enzymatically capped transcribed RNAs were then transfected into BSR-T7 cells and incubated for 48 hours for MNV-1 recovery. Virus yields were determined by

TCID50 and transfection efficiency was assessed using western blot analysis against MNV-1 NS7 protein.

Treatment of RAW 264.7 cells with MNV-1, oxLDL and PPARγ ligands

RAW 264.7 cells ($1.2x10^6$ cells/well) were grown in a 6-wells plate for 24 hours. Following 24 hours incubation, the cells were subjected to infection with MNV-1 at multiplicity of infection (m.o.i) of 0.01 and/or treatment with oxLDL (80 µg/ml) and/or ciglitazone (10 µM/ml), or 15dPGJ2 (5 µM/ml). The treated cells were further incubated at 37°C in 5% CO_2 incubator for 6, 12 and 24 hours before been harvested for subsequent assays.

PCR amplification of targeted MNV-1 subgenomic region

In order to verify MNV-1 infection in all respective treatments, the treated cells at 6, 12 and 24 hours were subjected to total RNA extraction using GenElute™ Mammalian Total RNA Miniprep Kit (ProMega, USA). A 0.5 ug of total RNA from all treated cells was reverse transcribed into cDNA using Tetro cDNA synthesis kit from Bioline, UK. For detection of MNV-1 subgenomic RNA, the forward primer 5′-GCAATTCCATCTCAAAT GTTCAAAACCTTCAGGCAAAC-3′ and reverse primer 5′-TTTTTTTTTTTTTTTTTTTTTTTTTTTTTTTAAAA TGCATCTAACTACCACAAAG-3′ were used. PCR was performed using MyCycler Thermal Cycler, BioRad (USA). The parameters used for PCR amplification were 95°C for 2 min, followed by 30 cycles consisting of denaturation at 95°C for 30 sec, annealing at 55°C for 30 sec and extension at 72°C for 1 min. The process of DNA extension was extended for another 1 min at the end of the last cycle. Ten µl of each PCR product was subjected to 0.8% agarose gel electrophoresis and was visualised under UV transiluminator.

Determination of MNV-1 titre by TCID50

MNV-1 titre in initial virus recovery experiment and subsequent experiments involving all types of treatments in RAW 264.7 cells at respective time points was determined by serial dilution of the virus in 96 well plates using antibiotic free DMEM as diluents. The dilutions of the virus ranged from 10^{-1} to 10^{-7} in 50 µl DMEM were overlayed with 1 x 104 BV-2 cells in 100 µl DMEM. Microscopic visualisation was used to view the appearance of cytopathic effect. Wells in each repeat titration were scored for cytopathic effect after 3-5 days. Viral titres were calculated using standard formula following Reed and Muench, 1938 (26).

Lipid droplet visualisation by Oil red O staining

Treated cells at respective time points were placed onto cover slides in the 6-well plates. Cells were then fixed with fixative solution (11 ml of 37% formaldehyde was added into 29 ml PBS) for 30 minutes followed by washing with PBS for two times. The cells were pre-treated with 60% 2-propanol for 15 seconds and then stained with 0.2% Oil red O (ORO)(Sigma) in 60% 2-propanol for 50 minutes. The slides were then washed with 2-propanol and followed by PBS. Then, cells were stained with Mayers hematoxylin (R&M, USA) for 1 minute to stain the nuclei. For visualisation, the stained lipid droplets were observed under light microscope at 40X magnification.

Cholesterol ester measurement

Treated cells were lysed in RIPA buffer (50 mM Tris pH 8.0, 150 mM NaCl, 1 mM EDTA, 1% Triton X-100 and 0.1% SDS) and CE content was quantified using Amplex Red Cholesterol Ester Measurement Kit (Invitrogen, USA). All of the reagents, cell lysate samples and standard controls (1 µg to 8 µg) were prepared based on manufacturer's instructions. Briefly, 50 µl of diluted sample (5 µl of lysate + 45 µl of 1x reaction buffer), blank control (1x reaction buffer) and standard controls were added into the wells of 96-well plate in triplicate. Then, 50 µl of the Amplex® Red reagent/HRP/cholesterol oxidase/cholesterol esterase working solution was added into each well containing sample, blank control or standard controls. The reactions were incubated for 30 minutes or longer at 37°C and protected from light. After incubation, absorbance reading of the sample was quantified using fluorescence microplate reader using excitation range of 530-560 nm and emission detection at ~590 nm.

Statistical analyses

The cholesterol ester content in the untreated and treated RAW 264.7 cells were subjected to statistical analysis by One-Way ANOVA followed by Bonferroni post-test using the GraphPad software version 8.0 by Prism. A p value of less than 0.05 is considered significant.

RESULTS

MNV-1 recovery produces significant titre of infectious recombinant virus

One of the main aims of this study was to assess the effect of MNV-1 infection in RAW 264.7 cells for the formation of foam cells as characterized by the accumulation of lipid droplets in the cytosol. In order to obtain the infectious MNV-1 particles, the RNA-based reverse genetics system for the recovery of virus was employed following the optimised method as described previously (30). Figure 1 shows the results for virus yield of the RNA-based MNV-1 recovery assay which is expressed as TCID50 per transfection of 1.5×10^6 cells. The purified-capped MNV-1 RNA transcripts were successfully produced *in vitro* and the integrity of these capped-RNA transcripts were examined with 0.8% agarose gel electrophoresis (Fig. 1a). Transfection of WT capped MNV-1 transcripts into BSRT7 cells has successfully produced 1.56×10^4 TCID50/ml per 1.5×10^6 cells virus but no detectable virus for F/S and ΔNS7 capped MNV-1 transcripts which act as controls for virus recovery assay (Fig 1b). Western blot analysis against MNV-1 NS7

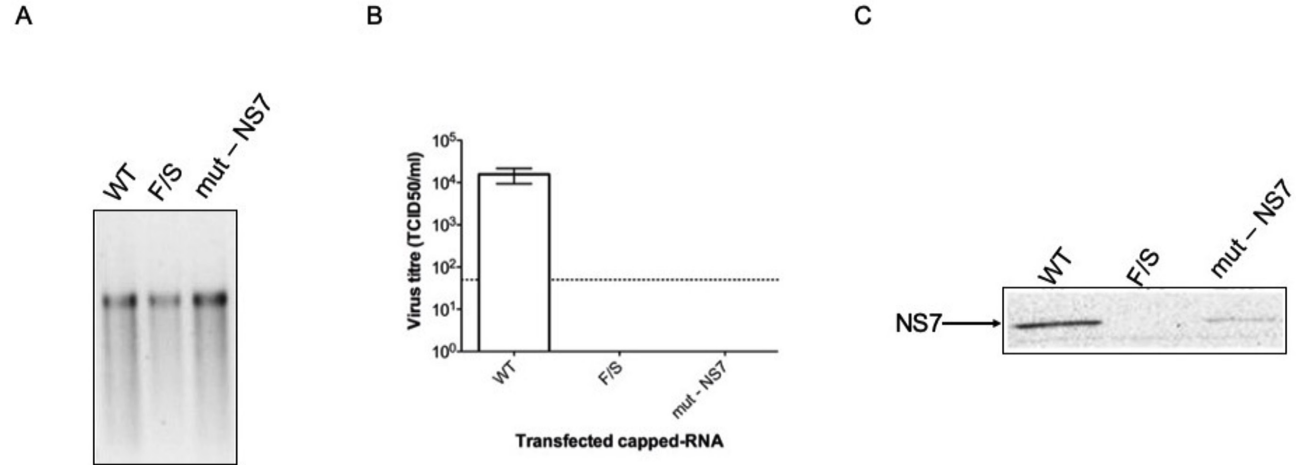

Figure 1: RNA-based recovery of MNV-1. Recombinant MNV-1 particles for this study were generated via RNA-based reverse genetics system as described previously by Yunus et al., (2010). (A) Analysis of MNV-1 capped-RNA transcripts integrity after purification on 0.8% agarose gel electrophoresis. Linearised plasmid cDNAs carrying MNV-1 genome (WT, F/S and mut-NS7) were subjected to in vitro transcription followed by *in vitro* enzymatic capping and purified using LiCl precipitation. (B) Titre of recovered MNV-1 particles from RNA-based reverse genetics system. Transfection with WT capped-transcripts produced 1.56 X 10^4 TCID50/ml virus particle while F/S and mut – NS7 capped transcript didn't produce any detectable virus. Discontinuous line on the bar chart represent detection limit of TCID50 which is 50 particles. (C) Western blot analysis targeting MNV-1 NS7 (RNA-dependent RNA polymerase). MNV NS7 protein bands at ~60 kDa were detected for WT and mut – NS7 samples.

showed that the transfected capped-RNA transcripts were successfully delivered into the cells and translated efficiently to produce viral protein (NS7) (Fig. 1c). The initially recovered MNV-1 from this RNA-based reverse genetics system was subjected to propagation in RAW 264.7 cells and verified for its infectivity using single step growth curve assay. Figure 2 shows the kinetics of replication for recombinant MNV-1 used in this study. The virus replication in RAW 264.7 cells peaked at 12 and 24 h.p.i as indicated by TCID50 data (Fig. 2a). The semi-quantitative PCR amplification analysis of MNV-1 specific genomic and sub-genomic region (Fig. 2b) also indicated that the viral RNA accumulation across the time points as a result of viral RNA replication. Western blot analysis (Fig. 2a) that was carried out on viral NS7 protein also found to be corresponded to the semi-quantitative PCR data whereby NS7 production was found to increase over time of infective incubation period. The infectious recombinant MNV-1 produced and characterised as above was subjected to further use in subsequent assays aimed at examining its effect in foam cell formation.

Formation of foam cells upon treatment with oxLDL on RAW 264.7 cells and effect of PPARγ ligands

To examine the uptake of oxLDL by RAW 264.7 cells, we quantitatively compared the CE content of the oxLDL-untreated RAW 264.7 cells (RAW) with oxLDL-treated RAW 264.7 cells (RAW+oxLDL) at 24 hours post treatment. There was almost more than 3-fold difference in CE content between the RAW and the RAW+oxLDL (Fig. 3b). Qualitative observation via Oil red O staining also demonstrated the accumulation of lipid droplets intracellularly over the incubation period

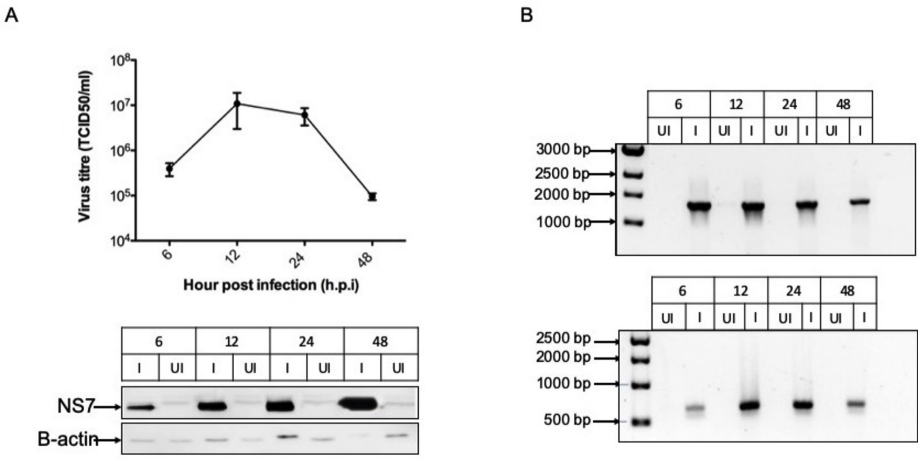

Figure 2: Characterisation of MNV-1 particles recovered from RNA-based reverse genetics system. (A) Top panel: Single-step growth curve of MNV-1 represented by virus titre using TCID50. RAW 264.7 cells were subjected to infection with the recovered MNV-1 previously at m.o.i of 1. TCID50 analysis at 4 different time points indicating robust and infective MNV-1 growth with peak titre obtained at 12 h.p.i. Bottom panel: Western blot analysis using antisera to MNV NS7 and β-actin against lysates from infected (I) and un-infected (UI) RAW 264.7 cells from the single-step growth curve assay. (B) Detection of MNV-1 genomic (G) RNA (top panel) and subgenomic (SG) RNA (bottom panel) as represented by PCR amplification of cDNA prepared from the total RNA extraction samples of the virus infected (I) and un-infected (UI) RAW 264.7 cells.

for the RAW+oxLDL (Fig. 3a). These data indicate that oxLDL treatment on RAW 264.7 cells stimulate the formation of foam cells. We also assessed the effect of PPARγ ligands treatment towards the formation of foam cells by specifically looking at the uptake of oxLDL and the accumulation of intracellular CE content of the treated RAW 264.7 cells. Our data showed that 15d-PGJ2 enhanced the oxLDL uptake by RAW 264.7 cells (Fig. 3a) and thus significantly increased the CE content intracellularly (Fig. 3b). However, ciglitazone had no significant effect on the formation of foam cells as the RAW+oxLDL+CIGLITAZONE treatment showed a similar CE content with RAW+oxLDL (Fig. 3b).

Combinatorial effect of MNV-1 infection and PPARγ ligands on formation of foam cells

In assessing potential contribution of MNV-1 infection on RAW 264.7 cells towards the formation of foam cells, we first inoculated the RAW 264.7 cells with MNV-1 (rescued from the RNA-based reverse genetics system above with two passages) at m.o.i of 0.01 then followed by treatment with oxLDL. Qualitative observation by lipid droplets staining method showed no clear increase in accumulation of lipid within the cells over the incubation period (Fig. 4a). This observation was further supported by quantification of CE content which revealed the non-significant reduction of intracellular cholesterol for RAW+oxLDL+MNV-1 in comparison to RAW+oxLDL (Fig. 4b). We further examined the effect of PPARγ ligands treatment on formation of foam cells derived from MNV-1 infected RAW 264.7 cells. For this purpose, the MNV-1 infected RAW 264.7 cells were subjected to treatment with oxLDL and ciglitazone or 15d-PGJ2. From visual observation by lipid staining, we found that the

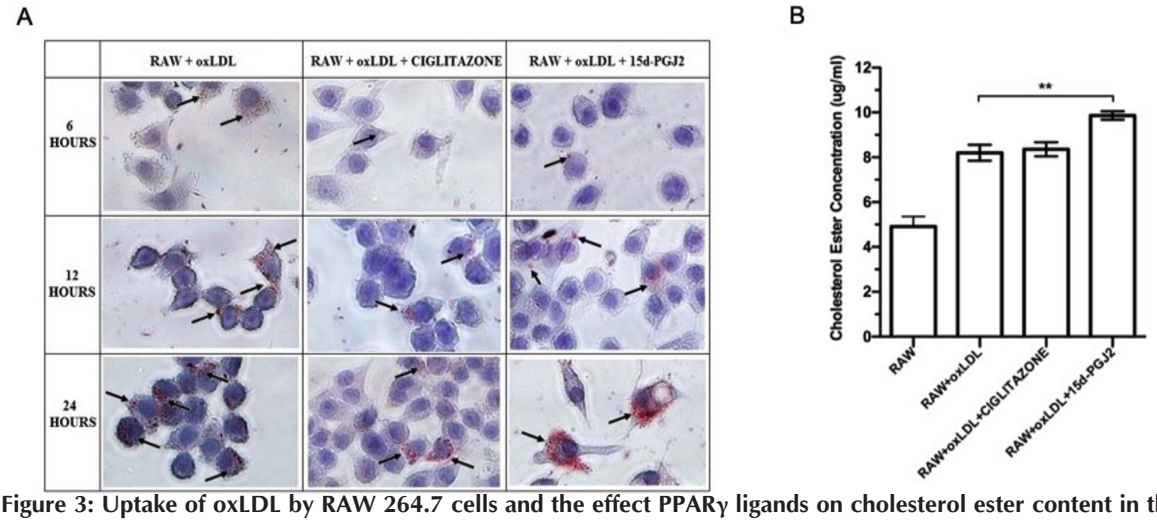

Figure 3: Uptake of oxLDL by RAW 264.7 cells and the effect PPARγ ligands on cholesterol ester content in the treated RAW 264.7 cells. (A) Microscopic visualisation of foam cell formation (ORO staining) in RAW+oxLDL, RAW+oxLDL+ciglitazone, RAW+oxLDL+15d-PGJ2 at 6, 12 and 24 hours. All the images were visualised under 40x magnifications. Lipid droplets (as pointed by arrow) were detected in all of the cell culture conditions at respective time points. (B) Quantification of CE content involving oxLDL and/or PPARγ ligands-treated RAW 264.7 cells at 24 hours post treatment. Statistical significance was determined using the ONE-WAY ANOVA with Bonferroni-post test, where $p < 0.05$. Error bar represents SD of three replicates.

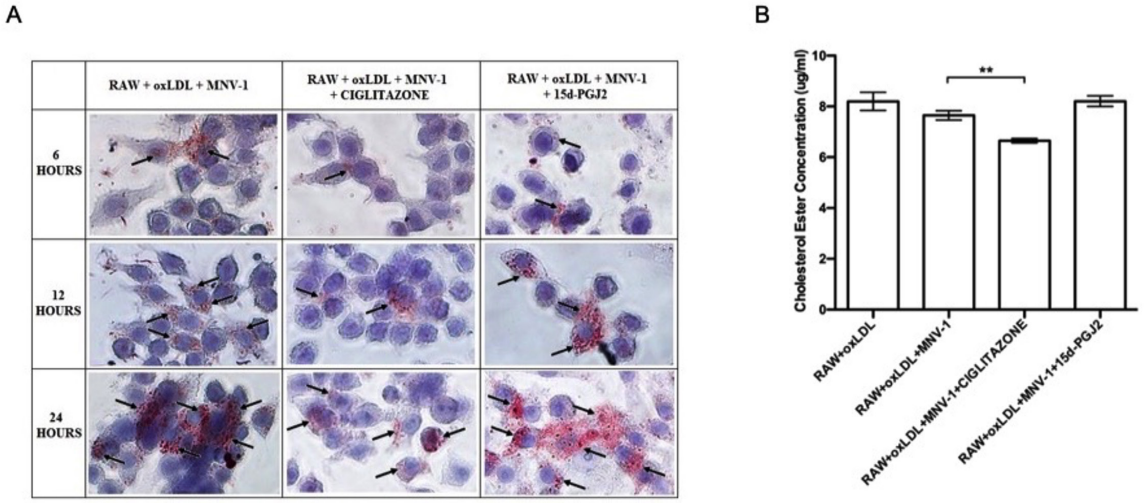

Figure 4: Effect of MNV-1 infection and PPARγ ligands treatment involving RAW 264.7 cells on foam cell formation. (A) Microscopic visualisation of foam cell formation in RAW+oxLDL+MNV-1, RAW+oxLDL+MNV-1+ciglitazone and RAW+oxLDL+MNV-1+15d-PGJ2 at 6, 12 and 24 hours. All the images were visualised under 40x magnifications. Lipid droplets (pointed by arrow) were detected in all of the cell culture conditions at respective time points. (B) CE content quantification of MNV-1 infected RAW 264.7 cells followed by treatment with oxLDL and respective PPARγ ligands at 24 hours post treatment. Statistical significance was determined using the ONE WAY ANOVA with Bonferroni-post test where $p < 0.05$. Error bar represents SD of three replicates.

lipid droplets of RAW+oxLDL+MNV-1+CIGLITAZONE was less compared to RAW+oxLDL+MNV-1+15d-PGJ2 and RAW+oxLDL+MNV-1 (Fig. 4a). Quantification of intracellular CE content also showed a significant reduction in CE for RAW+oxLDL+MNV-1+CIGLITAZONE compared to RAW+oxLDL+MNV-1 (Fig. 4b). This result suggests a synergistic effect of MNV-1 infection and ciglitazone treatment in hindering the uptake of oxLDL and/or reducing the intracellular cholesterol content. However, we did not see this intracellular CE content-reducing effect for RAW+oxLDL+MNV-1+15d-PGJ2 (Fig. 4b).

Effect of oxLDL and PPARγ ligands on MNV-1 replication

We also examined the effect of oxLDL and/or PPARγ ligands on MNV-1 replication in RAW 264.7 cells where all the treatments involved were subjected to RNA extraction, cDNA synthesis (on equal concentration of RNAs) and PCR amplification utilising the MNV-1 specific oligonucleotides that target the viral subgenomic region. This assay was also used to verify the presence of MNV-1 infection in all the treatments involved. In addition, we also carried out virus titration on all the treated samples to assess the virus replication. Our PCR amplification data showed the increased intensity of MNV-1 specific amplicons across the three time points (6, 12, and 24 hour) where RNA samples were collected (Fig. 5a). This data also confirmed the presence of MNV-1 infection in all the samples with virus inoculation compared to samples without virus inoculation. In addition, the TCID50 data at 24 h.p.i showed significant MNV-1 titre reduction when the infected-RAW 264.7 cells were treated with ciglitazone, indicating some inhibitory effect of this PPARγ ligands towards MNV-1 replication (Fig. 5b). This significant result was observed either in the presence of oxLDL or in the absence of oxLDL (RAW+MNV-1+oxLDL+CIGLITAZONE and RAW+MNV-1+CIGLITAZONE). In contrast, we found no significant effect of 15d-PGJ2 or oxLDL treatments alone on MNV-1 replication.

DISCUSSION

Possibility of infections in contributing to the development of atherosclerosis was suggested as early as 1800s and 1900s (27). MNV-4 infection has been shown to carry a potential in suppressing the ABCA1 transporter and increasing of CD36 expression (10, 11). MNV infection also has been shown to have no influence on glucose metabolism and weight gain, but it increased the size and macrophage content of aortic sinus lesions in Ldlr–/–mice fed with an atherogenic diet (10). It is also suggested that MNV-4 infection could potentially increases the oxLDL uptake capacity of macrophages since there was increased in CD36 protein expression (10). However in another study conducted by Hsu et al., (2015) there are variable influence of MNV-4 infection on the development of atherosclerosis whereby some of the data obtained suggested that the virus infection does not have any significant role in the development of atherosclerosis (11). This variable outcomes of MNV-4 infection in mice motivated us to further investigate a potential role of MNV in atherosclerosis but, using *in vitro* approach.

The introduction of reverse genetics system as a tool for the study of MNV and a small animal model have facilitated the investigation of viral sequences role in replication and pathogenesis of the diseases (28, 29). The availability of this technique also has enabled generation of recombinant virus from cloned viral genome in carrier plasmid. In the fields of norovirus molecular biology, two different approaches have been reported as a recovery method of genetically defined MNV. The first strategy involves both in vitro synthesis and capping of viral RNA known as RNA based virus recovery (30) whereas the second method involves the transcription of MNV cDNA in cells expressing T7 RNA polymerase or cDNA-based virus recovery (29, 31). Both systems reportedly to produced typical virus yield of >4 x 10^5 and >3 x 10^4 TCID50/35 mm dish respectively. In our study, we employed the RNA-based system and

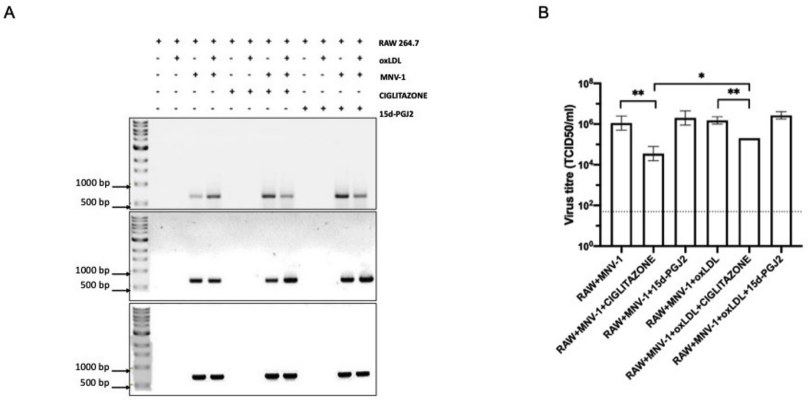

Figure 5: Effect of oxLDL and PPARγ ligands on MNV-1 replication in RAW 264.7 cells. (A) Verification of MNV1-infection in all culture conditions at respective time points (6 hour-top panel, 12 hour-middle panel, 24 hour-bottom panel) by PCR. Total RNA was extracted from all the culture conditions at all respective time points and subsequently subjected to cDNA synthesis. The cDNAs were subjected to PCR to amplify the MNV-1 subgenomic region (648 bp). (B) Virus titre analysis at 24 hours post infection using TCID50 method. All treated samples collected after 24 hours incubation were subjected to TCID50 assay. Statistical significance was determined using the ONE WAY ANOVA with Bonferroni-post test where $p< 0.05$. Error bar represents SD of three replicates.

obtained a virus yield of 1.56 x 10^4 TCID50/35 mm dish which were approximately 10-fold lower compared to the previously reported in Yunus et al., (2010). Even though the viral yield obtained in our study was lower compared to the previous studies, it was still considered as sufficient and we managed to further propagate the initially recovered MNV-1 in RAW 264.7 cells to get a higher virus titre for our subsequent experiments. High level of recovery yield in this study also was not crucial since the major aim was to produce infectious MNV-1 only.

The low passage recombinant MNV-1 was then used to infect the RAW 264.7 cells with or without oxLDL, ciglitazone and 15-dPGJ2 treatment to further investigate their involvement in atherogenesis. We used m.o.i of 0.01 TCID50 per cell for all RAW 264.7 cells treatment since our preliminary study using higher m.o.i resulted in apoptosis of the cells within 24 hours of post infection (data not shown). Moreover, m.o.i of 0.01 TCID50 per cell was sufficient to infect the RAW 264.7 cells as early as 6 hours whereby subgenomic RNA region of MNV-1 as well as viral titre could be determined. We targeted the partial viral subgenomic region in PCR amplification because detection of MNV subgenomic RNA always been used as indicative of active viral RNA genome replication. The reverse primer specifically targeting the 3'end of viral sequence including the 30 nucleotides polyA stretch together with forward primer at nucleotide position of 6733 in viral genome were used in PCR amplification. Currently, no studies have been carried out on the effect of PPARγ ligand on MNV-1 replication. Our results showed that inclusion of 15d-PGJ2 in MNV-1 infected RAW 264.7 cells consistently produced high level of virus titres irrespective of presence of oxLDL (Fig. 5b). Interestingly, low level of virus titres was recorded for ciglitazone-treated RAW 264.7 cells. These findings suggest that the natural PPARγ ligand, 15d-PGJ2 stimulates MNV entry/replication in the RAW 264.7 cells in comparison to PPARγ synthetic ligands, ciglitazone. These outcomes presumably be due to the differential structure of 15d-PGJ2 and ciglitazone. There were other reports showed that PPARγ agonists are capable of inhibiting HIV-1 replication in macrophages and T lymphocytes *in vitro* (32, 33). Moreover, other PPARγ synthetic ligand namely rosiglitazone was able to inhibit HIV-1 replication in human monocyte-derived macrophages (MDM) through the ability of PPARγ to inhibit NF-κB pathway which caused the down-modulation of HIV-1 LTR promoter activity leading to decrease in virus replication (34).

Our study also demonstrated that oxLDL treatment on MNV-1 infected RAW 264.7 cells (with the presence or absence of PPARγ ligands) consistently produced high titre virus compared to sample without oxLDL treatment. This finding indicates that oxLDL may influence the entry/replication of MNV-1 in RAW 264.7 cells. In support of this observation, studies on MNV entry into macrophages demonstrated that this virus specifically utilised a dynamin II and cholesterol- mediation mechanism (35, 36). In addition, extensive studies on hepatitis C virus (HCV) have shown that lipid droplets act as virion assembly localisation intracellularly with the involvement of viral proteins (37, 38). Thus, the high levels of intracellular-lipid droplet also presumably enhance virus replication.

The ORO staining is a well-known and established approach to evaluate foam cell formation in macrophages from various origins such as murine macrophage cell line RAW 264.7, J774 A.1, human THP-1, human monocyte-derived macrophages, bone marrow-derived macrophages and smooth muscle cells (39). It precisely dyes triglycerides and cholesteryl oleate (39). In our study, microscopic visualisation of the ORO stained cells, showed no lipid droplets were observed in the non-oxLDL treated samples (data not shown). Lipid droplets accumulation were only observed in all samples treated with oxLDL (Fig. 3a & 4a). These microscopic visualisations of the stained cells showed that oxLDL increased lipid droplet accumulation in macrophages as early as 6-hour post treatment until 24 hours. The morphological appearance of foam cells was as presented by ORO-stained lipid droplets which not only detected in the perinuclear area, but also appeared throughout the cytosol of most cells and this result also in agreement with the previous study by Xu et al., (2010). We also found that combination of oxLDL and MNV-1 infection increased foam cell formation because more lipid droplets (stained in red) were presence when compared to the oxLDL-treated RAW 264.7 cells without MNV-1 infection. The addition of PPARγ ligands (ciglitazone and 15d-PGJ2) also further increased lipid droplets accumulation which may suggest the stimulatory role of these ligands on the formation of foam cells.

Besides the uptake of cholesterol, the ratio of free cholesterol (FC) and CE is also important for the regulation of intracellular cholesterol content in macrophage derived foam cells. Following internalization of lipoproteins, they are transported to the late endosome/lysosome compartment in which CE is hydrolyzed into FC by lysosomal acid lipase (LAL) (4). In order to hinder the FC-associated cell toxicity, the FC released is re-esterified on the endoplasmic reticulum (ER) by ACAT1 and deposited in cytoplasmic lipid droplets (4). If this process continuously happens, excessive CE will assemble in macrophages which accelerating the formation of foam cells (4). In our study, all samples were subjected to quantitative CE content measurement to evaluate the correlation with microscopic visualisation of ORO stained results.

At 24 hours post treatments, analysis of our quantitative CE content data found that oxLDL treatment in RAW 264.7 in the presence of either ciglitazone or 15d-PGJ2

significantly increased CE level contents compared to non-oxLDL treated cells. This outcome was expected as overloading of oxLDL in macrophages stimulated the accumulation of CE stored as cytoplasmic lipid droplets and subsequently enhanced the formation of foam cells. Our result also demonstrated that MNV-1 did not increase CE contents in the oxLDL-treated RAW264.7 cells (Fig. 4b). Interstingly, this finding was in contradiction to previous *in vivo* study which showed that MNV-4 increased atherosclerotic lesion size and macrophage content in LDLr−/− mice and ApoE-/- fed a high fat diet (10, 11). However, MNV-4 is known to cause persistent infection in mice, whilst MNV-1 causes acute infection (17). The difference in persistency between MNV-1 and MNV-4 presumably influences the alteration of atherosclerosis development. In addition, in inbred immunocompetent mice, MNV-1 regulates a functioning STAT-1 pathway, which is important for interferon gamma (IFN-γ)-mediated signalling pathways (40). IFN-γ, initially known as macrophage-activating factor, plays a key role in the activation and homodimerisation of STAT-1 for target gene transcription (41). The important role of STAT-1 in IFN-γ and IFN-α/β signalling is demonstrated by using STAT-1-null mice and the mutant cell lines (42). Studies carried out on germline human STAT-1 mutation also showed that subjects with complete STAT-1 deficiency were more prone to viral and mycobacterial infections due to abolishment of STAT-1-dependent responses to both IFN-γ and IFN-α (43). IFNγ is highly expressed in atherosclerotic plaque and play a pivotal role in the atherosclerosis development (44). Our data showed that, unlike 15d-PGJ2, ciglitazone is working synergistically with MNV-1 to significantly reduce CE content in oxLDL-treated RAW 264.7 cells (Fig. 4b). Previous *in vivo* studies showed ciglitazone, 15d-PGJ2 and other PPARγ ligands treatment did not accelerate foam cell formation but give rise to the CD36 expression indicating that PPARγ could activate other pathways that can accelerate cholesterol efflux and reduce intracellular cholesterol level (45). Cholesterol efflux induction was mediated by transcriptional activation of PPARγ and liver X receptor α (LXRa) coupled with high expression of ABCA1, a protein transporter (46, 47). Our data suggests that PPARγ activation stimulates cholesterol efflux, thus enhancing the removal of oxLDL from the vessel wall. Moreover, the possible inhibition of IFNγ, a master regulator of atherogenesis by ciglitazone may support our findings (48). Therefore, given that the possible regulation of MNV-1 on the STAT-1 pathway functions which affect IFNγ we speculated that MNV-1 and ciglitazone synergistic effect in inhibiting IFNγ caused a significant reduced in the CE content. In contrast, we observed 15d-PGJ2 but not ciglitazone was able to increase CE content which enhanced foam cell formation. Our result was in accordance to the previous study which found 15d-PGJ2 in the cytoplasm of foam cell in human atherosclerotic plaque (49). These findings suggest that 15-dPGJ2 acts as a positive regulator in differentiation of macrophage into foam cells. However, this outcome was contradicted with studies by Matsuo et al., (2004) who revealed that 15d-PGJ2 suppressed oxLDL-induced macrophage proliferation by inhibiting GM-CSF secretion via NF-κB inactivation (50).

CONCLUSION

We successfully employed the RNA-based MNV-1 recovery method to produce infectious recombinant MNV-1 particles with relatively comparable yield with previous studies. OxLDL treatment towards RAW 264.7 cells consistently increased the intracellular CE content which indicative of foam cells formation. Interestingly, MNV-1 infection did not influence foam cells formation at least as observed *in vitro*. PPARγ ligands displayed different effects on intracellular CE content of oxLDL-treated RAW 264.7 cells as 15d-PGJ2 promote foam cells formation whilst ciglitazone inhibit the formation of foam cells and it worked synergistically with MNV-1 in distinct reduction of CE content. Ciglitazone also displays some degree of inhibition towards MNV-1 replication.

ACKNOWLEDGEMENTS

This research was supported by Fundamental Research Grant Scheme (FRGS), Ministry of Higher Education, Malaysia to M.A.Y (203/CIPPT/6711384). All the cDNA constructs for MNV-1 recovery and cell lines are obtained from Professor Ian Goodfellow, University of Cambridge, United Kingdom. K.M and R.M contributed equally in preparation of this manuscript.

REFERENCES

1. Tabas I, Garcнa-Cardeca G, Owens GK. Recent insights into the cellular biology of atherosclerosis. 2015.
2. Lusis AJ. Atherosclerosis. Nature. 2000;407(6801):233-41.
3. Colin S, Chinetti-Gbaguidi G, Staels B. Macrophage phenotypes in atherosclerosis. Immunological Reviews. 2014.
4. Yu X-H, Fu Y-C, Zhang D-W, Yin K, Tang C-K. Foam cells in atherosclerosis. Clinica chimica acta; international journal of clinical chemistry. 2013;424:245-52.
5. Blessing E, Campbell LA, Rosenfeld ME, Chough N, Kuo CC. Chlamydia pneumoniae infection accelerates hyperlipidemia induced atherosclerotic lesion development in C57BL/6J mice. Atherosclerosis. 2001;158(1):13-7.
6. Hayashi C, Viereck J, Hua N, Phinikaridou A, Madrigal AG, Gibson FC, 3rd, et al. Porphyromonas gingivalis accelerates inflammatory atherosclerosis in the innominate artery of ApoE deficient mice. Atherosclerosis. 2011;215(1):52-9.
7. Haidari M, Wyde PR, Litovsky S, Vela D, Ali

M, Casscells SW, et al. Influenza virus directly infects, inflames, and resides in the arteries of atherosclerotic and normal mice. Atherosclerosis. 2010;208(1):90-6.
8. Hsich E, Zhou YF, Paigen B, Johnson TM, Burnett MS, Epstein SE. Cytomegalovirus infection increases development of atherosclerosis in Apolipoprotein-E knockout mice. Atherosclerosis. 2001;156(1):23-8.
9. Cui HL, Grant A, Mukhamedova N, Pushkarsky T, Jennelle L, Dubrovsky L, et al. HIV-1 Nef mobilizes lipid rafts in macrophages through a pathway that competes with ABCA1-dependent cholesterol efflux. Journal of lipid research. 2012;53(4):696-708.
10. Paik J, Fierce Y, Mai P-O, Phelps SR, McDonald T, Treuting P, et al. Murine norovirus increases atherosclerotic lesion size and macrophages in Ldlr(-/-) mice. Comparative medicine. 2011;61(4):330-8.
11. Hsu CC, Paik J, Brabb TL, O'Brien KD, Kim J, Sullivan BG, et al. Murine Norovirus Infection Variably Alters Atherosclerosis in Mice Lacking Apolipoprotein E. Comparative medicine. 2015;65(5):369-81.
12. Karst SM, Wobus CE, Lay M, Davidson J, Virgin HWt. STAT1-dependent innate immunity to a Norwalk-like virus. Science. 2003;299(5612):1575-8.
13. Ward JM, Wobus CE, Thackray LB, Erexson CR, Faucette LJ, Belliot G, et al. Pathology of immunodeficient mice with naturally occurring murine norovirus infection. Toxicol Pathol. 2006;34(6):708-15.
14. Wobus CE, Thackray LB, Virgin HWt. Murine norovirus: a model system to study norovirus biology and pathogenesis. Journal of virology. 2006;80(11):5104-12.
15. Henderson KS. Murine norovirus, a recently discovered and highly prevalent viral agent of mice. Lab animal. 2008;37(7):314-20.
16. Hsu CC, Riley LK, Wills HM, Livingston RS. Persistent infection with and serologic cross-reactivity of three novel murine noroviruses. Comparative medicine. 2006;56(4):247-51.
17. Hsu CC, Riley LK, Livingston RS. Molecular characterization of three novel murine noroviruses. Virus genes. 2007;34(2):147-55.
18. Wobus CE, Karst SM, Thackray LB, Chang K-O, Sosnovtsev SV, Belliot G, et al. Replication of Norovirus in cell culture reveals a tropism for dendritic cells and macrophages. PLoS biology. 2004;2(12):e432-e.
19. Issemann I, Green S. Activation of a member of the steroid hormone receptor superfamily by peroxisome proliferators. Nature. 1990;347(6294):645-50.
20. Nagy L, Szanto A, Szatmari I, Szeles L. Nuclear hormone receptors enable macrophages and dendritic cells to sense their lipid environment and shape their immune response. Physiological reviews. 2012;92(2):739-89.
21. Tyagi S, Gupta P, Saini AS, Kaushal C, Sharma S. The peroxisome proliferator-activated receptor: A family of nuclear receptors role in various diseases. Journal of advanced pharmaceutical technology & research. 2011;2(4):236-40.
22. Duval C, Chinetti G, Trottein F, Fruchart J-C, Staels B. The role of PPARs in atherosclerosis. Trends in molecular medicine. 2002;8(9):422-30.
23. Li AC, Binder CJ, Gutierrez A, Brown KK, Plotkin CR, Pattison JW, et al. Differential inhibition of macrophage foam-cell formation and atherosclerosis in mice by PPARalpha, beta/delta, and gamma. The Journal of clinical investigation. 2004;114(11):1564-76.
24. Nagy L, Tontonoz P, Alvarez JG, Chen H, Evans RM. Oxidized LDL regulates macrophage gene expression through ligand activation of PPARgamma. Cell. 1998;93(2):229-40.
25. Cominacini L, Garbin U, Pasini AF, Davoli A, Campagnola M, Rigoni A, et al. The expression of adhesion molecules on endothelial cells is inhibited by troglitazone through its antioxidant activity. Cell Adhesion and Communication. 1999;7(3):223-31.
26. Reed LJ, Muench H. A SIMPLE METHOD OF ESTIMATING FIFTY PER CENT ENDPOINTS. American Journal of Epidemiology. 1938;27(3):493-7.
27. Prediman K. Shah MD. Link Between Infection and Atherosclerosis. Circulation. 2001;103:5-6.
28. Ward VK, McCormick CJ, Clarke IN, Salim O, Wobus CE, Thackray LB, et al. Recovery of infectious murine norovirus using pol II-driven expression of full-length cDNA. Proceedings of the National Academy of Sciences of the United States of America. 2007;104(26):11050-5.
29. Chaudhry Y, Skinner MA, Goodfellow IG. Recovery of genetically defined murine norovirus in tissue culture by using a fowlpox virus expressing T7 RNA polymerase. The Journal of general virology. 2007;88(Pt 8):2091-100.
30. Yunus MA, Chung LMW, Chaudhry Y, Bailey D, Goodfellow I. Development of an optimized RNA-based murine norovirus reverse genetics system. Journal of virological methods. 2010;169(1):112-8.
31. Arias A, Urena L, Thorne L, Yunus MA, Goodfellow I. Reverse Genetics Mediated Recovery of Infectious Murine Norovirus. Jove-Journal of Visualized Experiments. 2012(64).
32. Hayes MM, Lane BR, King SR, Markovitz DM, Coffey MJ. Peroxisome proliferator-activated receptor gamma agonists inhibit HIV-1 replication in macrophages by transcriptional and post-transcriptional effects. The Journal of biological chemistry. 2002;277(19):16913-9.
33. Roubenoff R, Grinspoon S, Skolnik PR, Tchetgen E, Abad L, Spiegelman D, et al. Role of cytokines and testosterone in regulating lean body mass and

resting energy expenditure in HIV-infected men. American journal of physiology Endocrinology and metabolism. 2002;283(1):E138-45.
34. Potula R, Ramirez SH, Knipe B, Leibhart J, Schall K, Heilman D, et al. Peroxisome proliferator-activated receptor-gamma activation suppresses HIV-1 replication in an animal model of encephalitis. AIDS (London, England). 2008;22(13):1539-49.
35. Perry JW, Wobus CE. Endocytosis of murine norovirus 1 into murine macrophages is dependent on dynamin II and cholesterol. Journal of virology. 2010;84(12):6163-76.
36. Gerondopoulos A, Jackson T, Monaghan P, Doyle N, Roberts LO. Murine norovirus-1 cell entry is mediated through a non-clathrin-, non-caveolae-, dynamin- and cholesterol-dependent pathway. The Journal of general virology. 2010;91(Pt 6):1428-38.
37. Miyanari Y, Atsuzawa K, Usuda N, Watashi K, Hishiki T, Zayas M, et al. The lipid droplet is an important organelle for hepatitis C virus production. Nature cell biology. 2007;9(9):1089-97.
38. Bartenschlager R, Penin F, Lohmann V, Andre P. Assembly of infectious hepatitis C virus particles. Trends in microbiology. 2011;19(2):95-103.
39. Xu S, Huang Y, Xie Y, Lan T, Le K, Chen J, et al. Evaluation of foam cell formation in cultured macrophages: an improved method with Oil Red O staining and DiI-oxLDL uptake. Cytotechnology. 2010;62(5):473-81.
40. Niendorf S, Klemm U, Mas Marques A, Bock CT, Hohne M. Infection with the Persistent Murine Norovirus Strain MNV-S99 Suppresses IFN-Beta Release and Activation of Stat1 In Vitro. PLoS One. 2016;11(6):e0156898.
41. Hu X, Chakravarty SD, Ivashkiv LB. Regulation of interferon and Toll-like receptor signaling during macrophage activation by opposing feedforward and feedback inhibition mechanisms. Immunological reviews. 2008;226:41-56.
42. Meraz MA, White JM, Sheehan KC, Bach EA, Rodig SJ, Dighe AS, et al. Targeted disruption of the Stat1 gene in mice reveals unexpected physiologic specificity in the JAK-STAT signaling pathway. Cell. 1996;84(3):431-42.
43. Dupuis S, Jouanguy E, Al-Hajjar S, Fieschi C, Al-Mohsen IZ, Al-Jumaah S, et al. Impaired response to interferon-alpha/beta and lethal viral disease in human STAT1 deficiency. Nature genetics. 2003;33(3):388-91.
44. Tellides G, Tereb DA, Kirkiles-Smith NC, Kim RW, Wilson JH, Schechner JS, et al. Interferon-gamma elicits arteriosclerosis in the absence of leukocytes. Nature. 2000;403(6766):207-11.
45. Ohshima K, Mogi M, Horiuchi M. Role of Peroxisome Proliferator-Activated Receptor-gamma in Vascular Inflammation. Int J Vasc Med. 2012;2012:508416.
46. Chawla A, Boisvert WA, Lee CH, Laffitte BA, Barak Y, Joseph SB, et al. A PPAR gamma-LXR-ABCA1 pathway in macrophages is involved in cholesterol efflux and atherogenesis. Molecular cell. 2001;7(1):161-71.
47. Chinetti G, Lestavel S, Bocher V, Remaley AT, Neve B, Torra IP, et al. PPAR-alpha and PPAR-gamma activators induce cholesterol removal from human macrophage foam cells through stimulation of the ABCA1 pathway. Nature medicine. 2001;7(1):53-8.
48. Cunard R, Eto Y, Muljadi JT, Glass CK, Kelly CJ, Ricote M. Repression of IFN-gamma expression by peroxisome proliferator-activated receptor gamma. Journal of immunology (Baltimore, Md : 1950). 2004;172(12):7530-6.
49. Shibata T, Kondo M, Osawa T, Shibata N, Kobayashi M, Uchida K. 15-deoxy-delta 12,14-prostaglandin J2. A prostaglandin D2 metabolite generated during inflammatory processes. The Journal of biological chemistry. 2002;277(12):10459-66.
50. Matsuo T, Matsumura T, Sakai M, Senokuchi T, Yano M, Kiritoshi S, et al. 15d-PGJ2 inhibits oxidized LDL-induced macrophage proliferation by inhibition of GM-CSF production via inactivation of NF-kappaB. Biochemical and biophysical research communications. 2004;314(3):817-23.